JACS
JOURNAL OF THE AMERICAN CHEMICAL SOCIETY
pubs.acs.org/JACS
Article

Electrosynthesis of Verdoheme and Biliverdin Derivatives Following Enzymatic Pathways

Amir Lashgari, Xiao Wang, Jeanette A. Krause, Soumalya Sinha,* and Jianbing "Jimmy" Jiang*

Cite This: J. Am. Chem. Soc. 2024, 146, 15955−15964
Read Online
ACCESS | Metrics & More | Article Recommendations | Supporting Information

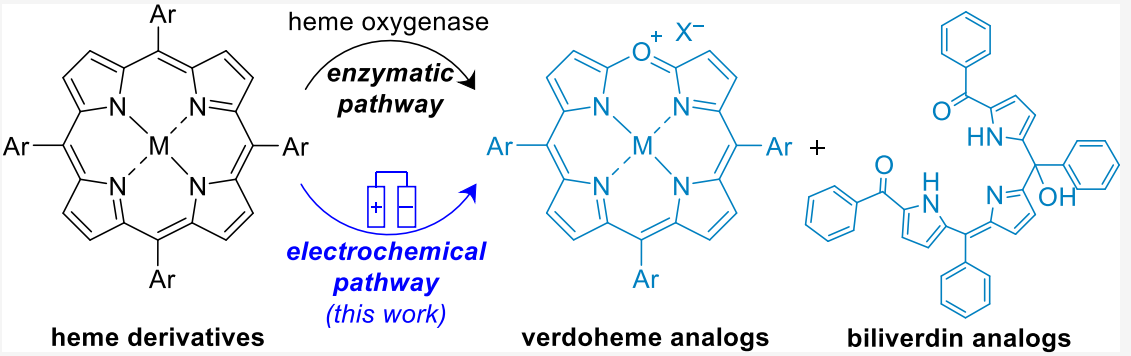

ABSTRACT: Artificial syntheses of biologically active molecules have been fruitful in many bioinspired catalysis applications. Specifically, verdoheme and biliverdin, bearing polypyrrole frameworks, have inspired catalyst designs to address energy and environmental challenges. Despite remarkable progress in benchtop synthesis of verdoheme and biliverdin derivatives, all reported syntheses, starting from metalloporphyrins or inaccessible biliverdin precursors, require multiple steps to achieve the final desired products. Additionally, such synthetic procedures use multiple reactants/redox agents and involve multistep purification/extraction processes that often lower the yield. However, in a single step using atmospheric oxygen, heme oxygenases selectively generate verdoheme or biliverdin from heme. Motivated by such enzymatic pathways, we report a single-step electrosynthesis of verdoheme or biliverdin derivatives from their corresponding meso-aryl-substituted metalloporphyrin precursors. Our electrosynthetic methods have produced a copper-coordinating verdoheme analog in >80% yield at an applied potential of 0.65 V vs ferrocene/ferrocenium in air-exposed acetonitrile solution with a suitable electrolyte. These electrosynthetic routes reached a maximum product yield within 8 h of electrolysis at room temperature. The major products of verdoheme and biliverdin derivatives were isolated, purified, and characterized using electrospray mass spectrometry, absorption spectroscopy, cyclic voltammetry, and nuclear magnetic resonance spectroscopy techniques. Furthermore, X-ray crystallographic data were collected for select cobalt (Co)- and Cu-chelating verdoheme and metal-free biliverdin products. Electrosynthesis routes for the selective modification at the macrocycle ring in a single step are not known yet, and therefore, we believe that this report would advance the scopes of electrosynthesis strategies.

INTRODUCTION

Bioinspired metal−ligand frameworks have motivated many catalyst designs, thus the synthesis of verdoheme or its derivatives is of interest.[1−3] In biological systems, heme oxygenase oxidizes heme into biliverdin through the formation of verdoheme, an iron-chelating β-alkyl-5-oxaporphyrin, by utilizing atmospheric dioxygen (Figure 1A).[4−8] Artificial syntheses of verdoheme and biliverdin ligand frameworks or their derivatives under chemical treatments have also been reported.[9−11] For example, Saito and Itano synthesized a verdoheme derivative, an iron-coordinating β-octaethyl-5-oxaporphyrin complex (**Fe-OEOxaPor**), by reacting a biliverdin derivative with acetic anhydride, pyridine, and iron sulfate, followed by treatment with sodium tetrafluoroborate (Figure 1B).[9] Balch et al. reported the **OEOxaPor** ligand chelated with a cobalt center; accomplished by oxidizing a Co(II)-coordinating β-octaethylporphyrin (**Co-OEPor**) in the presence of O_2 and ascorbic acid in a mixture of tetrahydrofuran and dichloromethane at −100 °C, followed by treatment with sodium dithionite and ammonium hexafluorophosphate (Figure 1B).[10] According to their observation, lowering the reaction temperature increased the local O_2 concentration and improved the overall reaction yield. Later in 2020, Takiguchi and co-workers reported a four-step synthesis of a metal-free **OEOxaPor** cation stabilized with a

Received: February 26, 2024
Revised: May 14, 2024
Accepted: May 16, 2024
Published: May 30, 2024

https://doi.org/10.1021/jacs.4c02847
J. Am. Chem. Soc. 2024, 146, 15955−15964

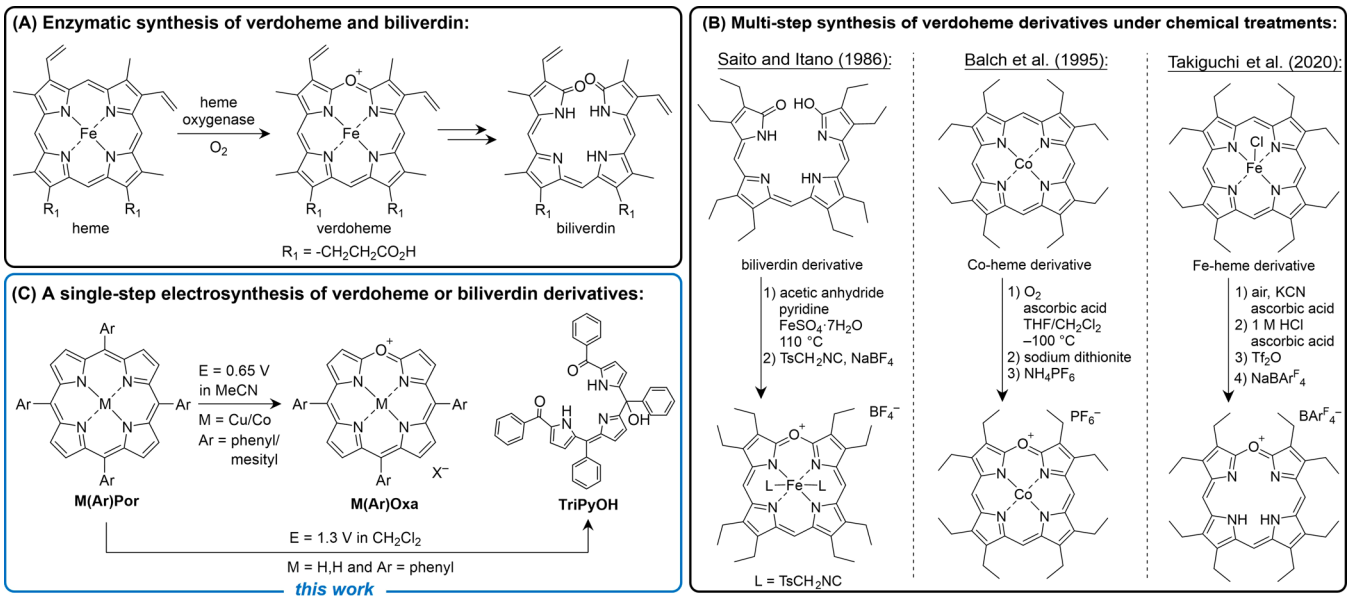

Figure 1. (A) Heme oxygenase catalyzes heme degradation to verdoheme and biliverdin production. (B) Synthetic models for the bioinspired verdoheme motif preparation through chemical treatments. (C) Selective electrosynthesis of verdoheme and biliverdin derivatives presented in this report.

nonpolar counterion prepared from an Fe(III)-centered octaethylporphyrin (Figure 1B).[11] However, the common drawback of these synthetic routes is that they involve multiple steps and require multiple chemical redox agents that are often toxic to the environment. In addition to the common drawbacks of the chemical synthesis, each chemical step of the multistep chemical synthesis protocols requires purification of the intermediate product before proceeding to the next chemical step, including solvent evaporation, product separation, and often recrystallization of the product that also reduces the overall yield of the final product.

While the abovementioned examples highlight artificial *β*-alkyl-5-oxaporphyrins syntheses, a few reported synthetic routes have also focused on the *meso*-arylporphyrins which have more straightforward synthetic routes, facile control of the electronic structure, and higher solubility of the former in nonpolar solvents.[12−15] A few such examples are the synthesis of first-row transition-metal coordinating *meso*-aryl-5-oxaporphyrins, where aryl groups are methyl carboxyphenyl or methoxy, but those synthetic procedures also require multiple chemical treatments to achieve the targeted final product.[16,17] A single-step synthetic route involving selective oxidation at the metalloporphyrin ring is desired for the selective synthesis of verdoheme and biliverdin derivatives. An electrochemical approach would benefit a variety of bioinspired syntheses, including verdoheme and biliverdin derivatives, and the typical sacrificial redox reagents could be avoided by tuning the applied potentials at the electrode.[18,19] However, reported electrochemical methods for the synthesis of macrocycles or selective modifications of macrocycle frameworks are rare. Herein, we report a single-step preparation of Cu(II) or Co(II) chelating *meso*-10,15,20-tri(aryl)-5-oxaporphyrins [**M(Ar)Oxa**, Ar = phenyl (Ph) or mesityl (Mes)] from the corresponding *meso*-5,10,15,20-tetraarylporphyrins [**M(Ar)Por**] by applying a constant potential of 0.65 V vs Fc/Fc^+ over 8 h under air (Figure 1C). The yields of such syntheses were high (>60%), and the desired counteranion was introduced directly from the supporting electrolyte, rather than through post-synthetic anion-exchange steps. Furthermore, the metal-free *meso*-5,10,15,20-tetraphenylporphyrin (**H_2PhPor**) was also treated under a constant applied potential of 1.3 V vs Fc/Fc^+ to produce biliverdin derivatives, and 1,14-dibenzoyl-5,10-diphenyl-tripyrrinone (**TriPyOH**) was obtained as the major product (79% yield, Figure 1C).

RESULTS AND DISCUSSION

The metalloporphyrin precursors, **MPhPor**, (M = Mn, Fe, Co, Ni, or Cu) were prepared by metalating the **H_2PhPor** ligand following literature methods (Table 1).[20,21] Controlled-potential electrolysis (CPE) was performed in MeCN solution with 0.1 M tetrabutylammonium hexafluorophosphate ($TBAPF_6$) or lithium bis(trifluoromethane)sulfonimide (LiTFSI) electrolyte. General methods and procedures are provided in the Experimental Section and Supporting Information. All CPE experiments were carried out under air unless otherwise noted. Ferrocene was used as an external standard.

Table 1. Applied Potential, Counterion, and Yield Obtained in the Electrosynthesis of MPhOxaX from MPhPor

MPhPor	$E_{applied}$ (V)	X	yield of MPhOxaX
MnPhPor	0.65 (for 8 h)	PF_6	unsuccessful
FePhPor	0.65 (for 8 h)	PF_6	unsuccessful
CoPhPor	0.95 (for 8 h)	TFSI	73%
NiPhPor	0.65 (for 8 h)	PF_6	unsuccessful
CuPhPor	0.65 (for 8 h)	PF_6	63%
	0.85 (for 8 h)	PF_6	52%
	1.0 (for 8 h)	PF_6	46%
	1.0 (for 2 h)	PF_6	28%
	1.0 (for 18 h)	PF_6	15%
	0.65 (for 8 h)	TFSI	82%

https://doi.org/10.1021/jacs.4c02847
J. Am. Chem. Soc. 2024, 146, 15955−15964

ELECTROSYNTHESIS OF VERDOHEME AND BILIVERDIN ANALOGS

Mimicking the Fe center of heme, initial investigations began with the preparation of **FePhOxa** from **FePhPor** (Scheme 1).

Scheme 1. Single-Step Electrosynthesis of Verdoheme Derivatives, MPhOxaX from MPhPor under Air

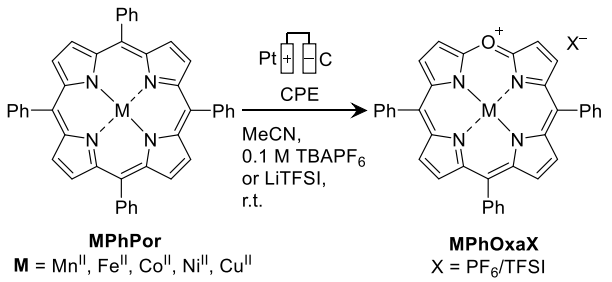

The CPE experiment was first tested for **FePhPor** by applying a constant potential at 0.65 V vs Fc/Fc^+ in MecN containing 0.1 M $TBAPF_6$ electrolyte over 8 h. The post-CPE solutions were checked by collecting UV−visible absorption spectra, and no new peaks were observed between 600 and 700 nm indicative of **FePhOxa**, as reported for the synthetic verdoheme derivative by Liu et al.[22] Attempts to synthesize **FePhOxa** from **FePhPor** were unsuccessful under the electrochemical conditions presumably due to the tendency of **FePhPor** to form triphenylbilindione and tetraphenylbiladienone while reacting with O_2.[17] To extend the scope of this study, we explored a series of **MPhPor** using additional first-row transition metals, M = Mn, Co, Ni, and Cu (Scheme 1). We also tested diamagnetic metalloporphyrin precursors, **MgPhPor** and **ZnPhPor**; however, the formation of desired products was not observed in the UV−visible spectra and thin-layer chromatography (TLC) over the course of bulk electrolysis (Figures S1 and S2). This could be due to the poor stability of the corresponding 5-oxaporphyrin derivatives. Interestingly, the Co and Cu complexes showed the formation of **CoPhOxa** and **CuPhOxa**, respectively, under the applied CPE conditions in the MeCN electrolyte for 8 h (Table 1). All further discussion herein is focused explicitly on these complexes. In addition, we studied the effects of applied potential, supporting electrolytes, bulkiness of the pendant groups at the meso-positions of the metalloporphyrin precursors, and the presence of water in the electrolyte solution on the final product yields.

Effects of the Applied Potential ($E_{applied}$) in CPE. The electrolyte solution (initially suspension) containing **CuPhPor** showed a prominent color change to purple-brown, followed by green during CPE at 0.65 V vs Fc/Fc^+ for 8 h in MeCN with $TBAPF_6$ as the electrolyte. The post-CPE solution was then collected, and the reaction mixture was separated using column chromatography to afford **CuPhOxaPF$_6$** in 63% yield (Table 1). The **CuPhOxaPF$_6$** product was characterized using electrospray ionization mass spectrometry (ESI-MS) and absorption spectroscopy techniques. Identical CPE experiments performed at more positive potentials, 0.85 and 1.0 V vs Fc/Fc^+ for **CuPhPor**, yielded comparatively lower amounts of the **CuPhOxaPF$_6$**, 52 and 46%, respectively (Table 1). Furthermore, CPE carried out for longer than 8 h did not increase the amount of **CuPhOxaPF$_6$** produced under the same electrochemical conditions (Table 1). We hypothesized that longer CPE experiments or application of high potentials, >0.65 V vs Fc/Fc^+, could lead to the demetalation of the metal complex, producing undesired side products. To test our hypothesis, we performed CPE for the metal-free **H$_2$PhPor** at 1.3 V vs Fc/Fc^+ for 18 h in CH_2Cl_2 containing 0.5 M $TBAPF_6$ (**H$_2$PhPor** is poorly soluble in MeCN). Such electrolysis experiments yielded three different derivatives of biliverdin, **TriPyOH**, ***α*TetPy**, and ***β*TetPy** (Scheme 2), in which **TriPyOH** was the major product (79% yield). **TriPyOH** was fully characterized by typical spectroscopic techniques such as

Scheme 2. Electrochemical Oxidation of H_2PhPor at 1.3 V vs Fc/Fc^+ in CH_2Cl_2 with 0.5 M $TBAPF_6$

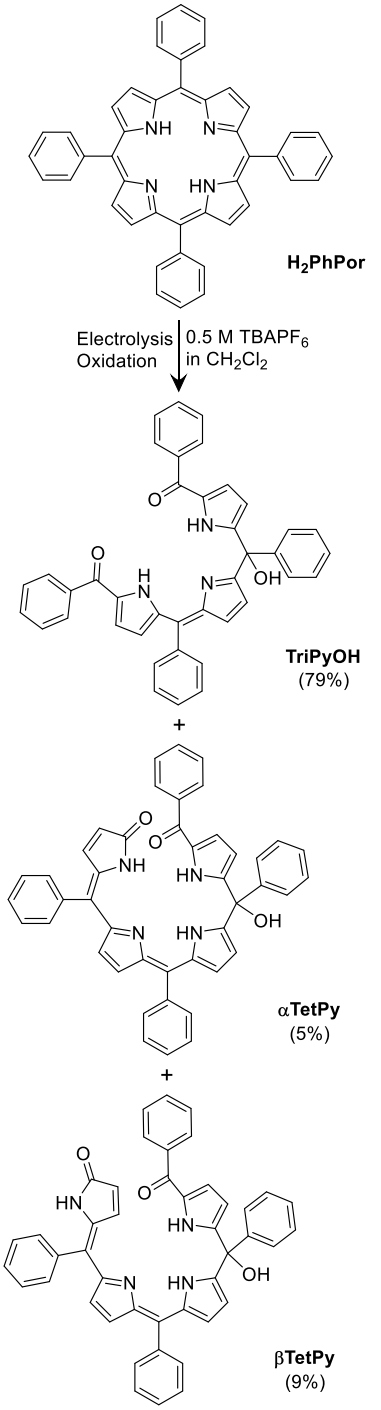

https://doi.org/10.1021/jacs.4c02847
J. Am. Chem. Soc. 2024, 146, 15955−15964

^{1}H and ^{13}C nuclear magnetic resonance (NMR) and ESI-MS. The structures of **CuPhOxaPF$_6$** and **TriPyOH** were confirmed using single-crystal X-ray diffraction (XRD).

To investigate the electrochemical processes facilitated by **CuPhPor** and **CoPhPor** at the applied potentials used in the CPE, 0.65 and 0.95 V vs Fc/Fc$^+$, respectively, we performed spectroelectrochemistry experiments using UV−visible spectroscopy while running CPE at those potentials. For **CuPhPor**, the spectral changes in the Soret and Q bands decrease over time (Figure S3A), indicating the formation of porphyrin π-cation radical under the oxidative condition.[23] On the contrary, the spectral changes of **CoPhPor** during the CPE were different and more indicative of the metal-centered oxidation processes, as reported in the literature (Figure S3B).[24]

Faradaic yields were also estimated for the electrosynthesis of **CuPhOxaTFSI** and **CoPhOxaTFSI**. Over 8 h of the CPE experiments, a total of 43.6 and 18 C of charges were passed during the electrosynthesis of **CuPhOxaTFSI** and **CoPhOxaTFSI**, respectively. Considering 43.6 C of charge during the electrosynthesis of **CuPhOxaTFSI**, we estimated the moles of electrons, 4.52×10^{-4} mol, which would provide 1.51×10^{-4} mol **CuPhOxaTFSI** theoretically. However, 2.98×10^{-5} mol pure **CuPhOxaTFSI** was obtained after purifying the post-CPE solution, which led to the Faradaic efficiency (FE) of 19.7%. Interestingly, a higher FE of 43.1% for the formation of **CoPhOxaTFSI** was achieved when the CPE was performed at 0.95 V vs Fc/Fc$^+$. However, the total charge passed during the electrosynthesis of **TriPyOH** from the free-base **H$_2$PhPor** in CH_2Cl_2 containing 0.1 M of $TBAPF_6$ was much lower, 6 C over 18 h of the electrolysis.

Effects of the Electrolyte. Surprisingly, the yield of the electrochemical oxidation of **CuPhPor** to [**CuPhOxa**]$^+$ increased from 63 to 82% when 0.1 M LiTFSI was used as the electrolyte. Such enhancements in yield may be explained by considering the molecular structure of **CuPhOxaTFSI** that reveals coordination of the TFSI to the Cu center (Figure 2), thus providing added stability to the complex. Similar results were observed for **CoPhPor**, at 0.95 V vs Fc/Fc$^+$ in 0.1 M LiTFSI in MeCN, producing **CoPhOxaTFSI** (Table 1). The molecular structure of this Co-verdoheme analog also exhibited similar TFSI coordination at the Co center (Figure 2). We also fully characterized **CoPhOXaTFSI** using NMR, ESI-MS, and UV−visible spectroscopy (see the Experimental Section).

Effects of the Bulkiness of the Meso-Substituents. The effects of the bulkiness of the meso-substituents on the porphyrin were studied by introducing different functional groups such as mesityl in the meso positions (Scheme 3). For example, electrolysis of **CuMesPor** under the optimal conditions using LiTFSI as the supporting electrolyte resulted in the isolation of **CuMesOxaTFSI** in 67% yield (Table 2), lower than that of **CuPhOxaTFSI** (82%). Changing the electrolyte to $TBAPF_6$ did not show a significant difference in the yield of **CuMesOxaPF$_6$** (Table 2). Two additional Cu porphyrin precursors, **Cu(CF$_3$)Por** and **Cu(OMe)Por**, were investigated under identical optimal CPE conditions (Scheme 3, Table 2). The electrosynthesis reaction of **Cu(CF$_3$)Por** resulted in a material with a peak observed at 648 nm in the UV−visible spectrum, suggesting the formation of the 5-oxaporphyrin product (Figure S4). The product proved to be unstable and decomposed during purification by column chromatography. On the contrary, electrolysis of **Cu(OMe)-Por** showed no desired product formation by UV−visible

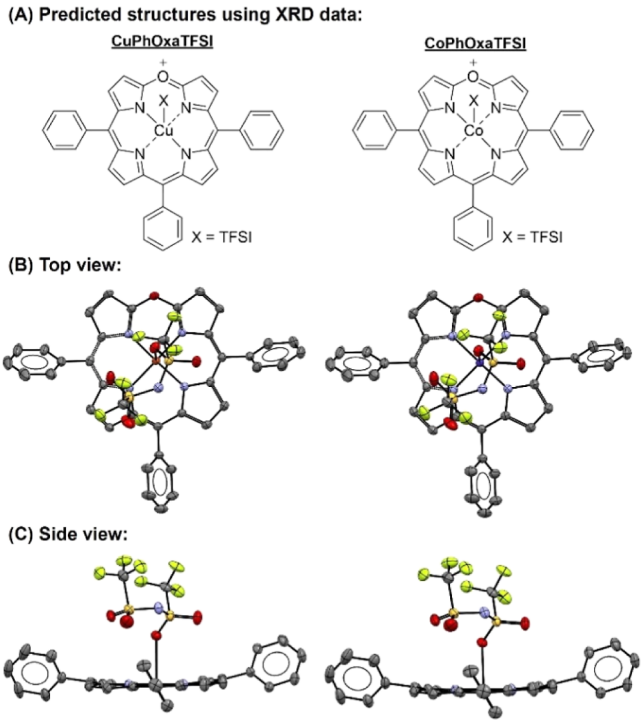

Figure 2. (A) Structures of TFSI coordinating **CuPhOxaTFSI** (left) and **CoPhOxaTFSI** (right) based on the XRD data, (B) top view, and (C) side view of the molecular structures of **CuPhOxaTFSI** and **CoPhOxaTFSI** with ellipsoids set at 50% probability. Only one independent molecule for **CuPhOxaTFSI** and **CoPhOxaTFSI** is shown. The distance between the metal center and the coordinated TFSI oxygen for the two independent molecules of **CuPhOxaTFSI** and **CoPhOxaTFSI** is $Cu_1\cdots O_{5TFSI}$ = 2.5859 (21), $Cu_2\cdots O_{8TFSI}$ = 2.5347 (22) Å and $Co_1\cdots O_{5TFSI}$ = 2.3543 (15), $Co_2\cdots O_{8TFSI}$ = 2.3147 (15) Å.

Scheme 3. Electrosynthesis of Cu-Verdoheme Derivatives Using Different *meso*-Aryl Substituents

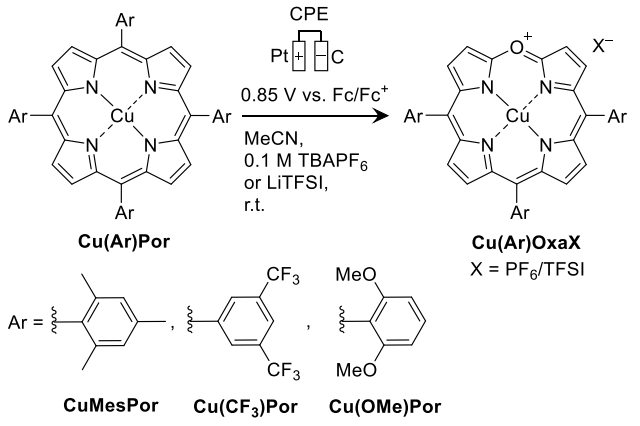

Table 2. Yield of Cu(Ar)OxaX (X = PF$_6$/TFSI) from Cu(Ar)Por Precursors

Cu(Ar)Por	yield of product
CuMesPor	64% CuMesOxaPF$_6$
	67% CuMesOxaTFSI
Cu(CF$_3$)Por	product detected by UV−vis, but unstable
Cu(OMe)Por	no product detected

https://doi.org/10.1021/jacs.4c02847
J. Am. Chem. Soc. 2024, 146, 15955−15964

spectroscopy and TLC, although all starting materials were consumed during the oxidation. Furthermore, synthesis of the metal-free verdoheme was also attempted using **H_2PhPor**, but our attempts were unsuccessful.

To understand the coordination chemistry of the Cu or Co-centered verdoheme derivatives, XRD data obtained for **CuPhOxaTFSI**, **CoPhOxaTFSI**, and **CuMesOxaPF$_6$** were analyzed. Crystallographic analysis showed that for both independent molecules of **CuPhOxaTFSI** and **CoPhOxaTFSI**, the O atom of the TFSI anion coordinates with the metal center of the 5-oxaporphyrinium cation (Figure 2), whereas for **CuMesOxaPF$_6$**, the PF_6 anion does not (Cu···F = 3.0−3.9 Å, Figures 3 and S5). Instead, the PF_6 anion and cocrystallized

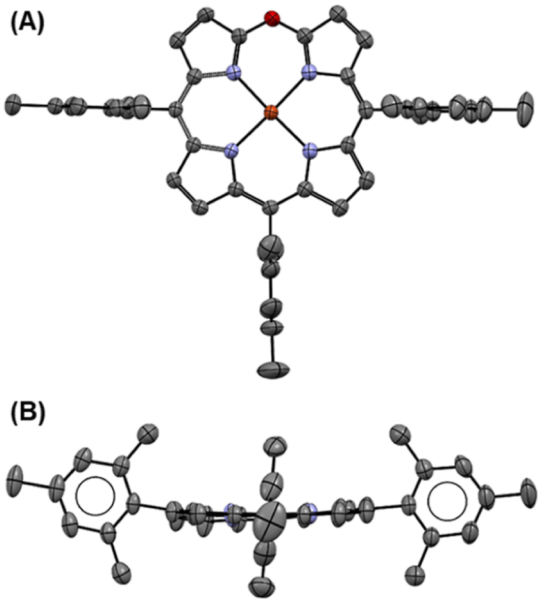

Figure 3. Molecular structures of **CuMesOxaPF$_6$** with ellipsoids set at 50% probability (A) top view and (B) side view. H atoms, the PF_6 anion, and the $CHCl_3$ solvate are omitted for clarity.

$CHCl_3$ molecules are disordered over two positions related by symmetry. The distances of the Cu−O_{TFSI} bonds (∼2.5 Å) are 0.2 Å longer than the Co−O_{TFSI} bonds (∼2.3 Å). For comparison, the reported *meso*-triphenyl-21,23-didehydro-23*H*-5-oxaporphyrinato]zinc(II) complex (**ZnOxaPor**) exhibits an axially coordinated interaction with the O atom of CF_3COO, the Zn−O bond length is 2.010 (4) Å.[12] The metal center in the Zn-complex adopts a dome shape, the Zn is situated 0.49 Å out of the nitrogen plane, whereas the cores of both **CuPhOxaTFSI** and **CuMesOxaPF$_6$** are essentially planar (the metal displacement is <0.1 Å). The dihedral angles C(pyrrole α)−C(*meso*)−C(phenyl *ipso*)−C(phenyl *ortho*) for **CuPhOxaTFSI** and **CoPhOxaTFSI** are between 56 and 62°, similar to that of **ZnOxaPor** (60−66°). However, for **CuMesOxaPF$_6$**, the corresponding angles are between 83 and 89°, which highlights the steric requirement of the mesityl groups. The dihedral angle for **CuPhPor** is 72°, and the compound adopts tetragonal symmetry.[25] The M−N bond lengths are given in the 1.965 (3)−1.991 (2) Å range for both independent molecules of the **CuPhOxaTFSI** and the **CuMesOxaPF$_6$** complexes; while the Co−N distances for **CoPhOxaTFSI** appear at slightly longer distances [1.945 (2)−1.960 (2) Å]. The bond distances of the carbon atoms adjacent to the O atom of the 5-oxaporphyrin ring for the complexes are reported as follows: **CuPhOxaTFSI**: 1.337 (4)−1.351 (3) Å; **CoPhOxaTFSI**: 1.334 (3)−1.341 (2) Å; and **CuMesOxaPF$_6$**: 1.336 (4), 1.345 (4) Å that fall within the range exhibited for **ZnOxaPor** [1.335(7) and 1.364(7) Å]. The C−O−C bond angles for **CuPhOxaTFSI**, **CoPhOxaTFSI**, and **CuMesOxaPF$_6$** fall in the 123.0−124.4° range and are consistent with **ZnOxaPor** (124.9°). In comparison, the distance between O and adjacent carbons in the 5-oxaporphyrinium ring for the cobalt β-octaethyl-5-oxaporphyrin complex with the PF_6 pairing anion was reported[10] to be 1.340 (6) and 1.348 (8) Å, with an angle of 124.8°.

Crystal packing diagrams with polyhedra about the Cu and Co metal centers for **CuPhOxaTFSI**, **CoPhOxaTFSI**, and **CuMesOxaPF$_6$** are shown in Figure 4. **CuPhOxaTFSI** and **CoPhOxaTFSI** crystallize in the triclinic crystal system, whereas **CuMesOxaPF$_6$** adopts a monoclinic arrangement, showing that **CuMesOxaPF$_6$** adopts a more symmetrical motif than **CuPhOxaTFSI** and **CoPhOxaTFSI**. The coordination polyhedron is defined by the cation−anion interactions around the central atom.[25] Given the coordination of the TFSI anion to the metal center, the geometry about the Cu and Co metal

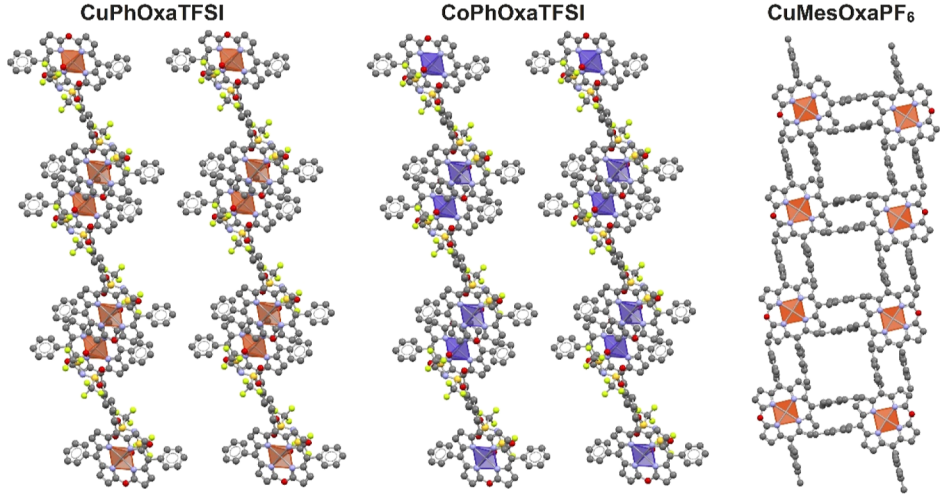

Figure 4. Crystal packing diagram with polyhedra around the copper metal center.

https://doi.org/10.1021/jacs.4c02847
J. Am. Chem. Soc. 2024, 146, 15955−15964

centers of **CuPhOxaTFSI** and **CoPhOxaTFSI** are tetrahedral while a planar arrangement is observed for **CuMesOxaPF$_6$** (Figure 4). In **CuPhOxaTFSI** and **CoPhOxaTFSI**, TFSI coordinates through one O atom of the sulfonyl group, presumably this binding mode is more stable than coordination with the N atoms.[26,27] In each layer, the dominant central copper-to-copper distances for **CuPhOxaTFSI** and **CuMesOxaPF$_6$** are 8.55 and 8.67 Å, respectively, and these distances are slightly longer than the shortest cobalt−cobalt distance in **CoPhOxaTFSI** of 8.51 Å.

Effects of O_2 and H_2O on the Yield. Under optimal electrolysis conditions using air as the reactant, both O_2 and H_2O (moisture) can participate in oxaporphyrin formation; therefore, it is necessary to determine the role of both species in oxaporphyrin formation. Two experiments were designed: (1) H_2O-free in the presence of O_2 and (2) O_2-free in the presence of H_2O. In each experiment, **CuPhPor** was used as the starting material and 0.1 M LiTFSI in MeCN as the electrolyte solution. The reactions were performed at 0.65 V vs Fc/Fc^+ for 8 h. In the first experiment, anhydrous MeCN was used as the solvent, and the working and counter electrolyte solutions were deaerated by bubbling with argon for 1 h before supplying pure oxygen gas for electrolysis. After chromatographic purification, an isolated yield of 90% was obtained. In the second experiment, after 1 h of degassing the electrolyte solution with argon, predegassed deionized H_2O (4 M) was added. Monitoring the color change during the CPE experiments, TLC profile, and UV−visible spectra suggested no detectable product in the post-CPE solutions. Finally, the need for an applied potential was confirmed using the reaction conditions employed in the first experiment, but without applying a potential to the electrolyte solution, and no product was formed even in the presence of pure O_2 gas. It was concluded that O_2 and the applied potential are key factors in the formation of 5-oxaporphyrin. Compared with that obtained using air, the yield of the reaction using pure O_2 gas increased slightly from 84 to 90%, indicating that the O_2 concentration had a minor effect on the kinetics of oxaporphyrin formation.

CPE in Undivided Cells. While the abovementioned results were obtained using a divided H-cell setup, where the working cell and counter cells are separated by a glass frit, an undivided cell provides a relatively simple cell setup and avoids the ohmic resistance that might occur in the presence of the glass frit. The benchmark compound, **CuPhPor**, was used for the study in an undivided cell. A faster reaction rate was observed, and a comparable yield of 84% was obtained within 5 h using the undivided cell at 0.65 V vs Fc/Fc^+, relative to 82% within 8 h for the divided cell.

PROPERTIES OF ELECTROCHEMICALLY SYNTHESIZED CU AND CO-VERDOHEME DERIVATIVES

Optical Properties. The UV−visible spectra were recorded for the electrochemically synthesized **CuPhOxaTFSI** (Figure 5A), **CoPhOxaTFSI** (Figure S6), **CuMesOxaTFSI** (Figure S7), and **CuMesOxaPF$_6$** (Figure S8). The absorption spectra revealed a very distinct change in the absorption maxima between metalloporphyrin precursors and verdoheme products. For example, the comparative absorption spectra of **CuPhPor** and **CuPhOxaTFSI** (Figure 5A) show significantly different absorption maxima. In general, all 5-oxaporphyrin complexes possess a characteristic B-band in the UV-violet region and an intensified Q-band in the red region. Mizutani et al. discussed two possible mechanisms for the intensified Q-band by comparing corresponding porphyrins: (1) removal of the degeneracy of the frontier orbitals of the porphyrins by replacing the meso carbon with oxygen and (2) an increase in the electric dipole moment by polarization because of the oxygen in the meso position.[12]

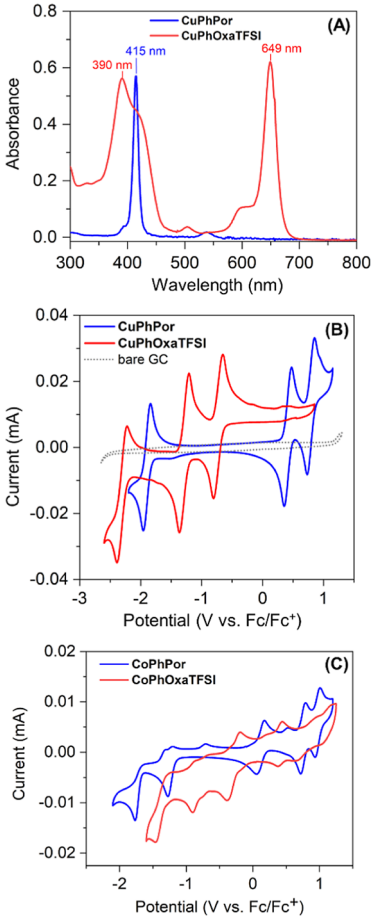

Figure 5. (A) UV−visible spectra of **CuPhPor** (blue) and **CuPhOxaTFSI** (red) recorded in CH_2Cl_2. Comparative CVs recorded for (B) **CuPhPor** (blue) and **CuPhOxaTFSI** (red) and (C) **CoPhPor** (blue) and **CoPhOxaTFSI** (red) in 0.1 M $TBAPF_6$ in CH_2Cl_2 as the electrolyte under N_2. CV collected for the bare glassy carbon (GC, gray) electrode is also shown for the comparison. The concentration of the compound used in the UV−visible and CV experiments is 28 μM and 5 mM, respectively.

Electrochemical Properties. The electrochemical properties of the synthesized Cu or Co-verdoheme analogs were also evaluated using cyclic voltammetry (Table 3). The cyclic voltammograms (CVs) of **CuPhOxaTFSI** (Figure 5B), **CuMesOxaTFSI** (Figure S9), and **CuMesOxaPF$_6$** (Figure S10) were collected in 0.1 M $TBAPF_6$ in CH_2Cl_2, and all of these electrosynthesized Cu-verdoheme derivatives exhibited reversible redox couples at approximately −0.7 and −1.3 V vs Fc/Fc^+. In comparison, these redox features are significantly different than that of their corresponding metalloporphyrin precursors (Figure 5B). The CV of **CuPhOxaTFSI** showed an additional quasi-reversible wave at −2.3 V vs Fc/Fc^+, which was not observed for **CuMesOxaTFSI** and **CuMesOxaPF$_6$**.

To understand the influence of the applied potential in the selective oxidation of the porphyrin ligand in **CuPhPor**, we recorded the CVs of **CuPhPor** in CH_2Cl_2 containing 0.1 M

https://doi.org/10.1021/jacs.4c02847
J. Am. Chem. Soc. 2024, 146, 15955−15964

Table 3. Half-Wave Potentials (V vs Fc/Fc^+) of Cu and Co Complexes in CH_2Cl_2 Containing 0.1 M $TBAPF_6$

complex	$E_{1/2}$ (V vs Fc/Fc^+)
CuPhPor	−1.89, 0.41, 0.79
CuPhOxaTFSI	−2.31, −1.29, −0.76
CuMesPor	−2.09, 0.35, 0.79
CuMesOxaTFSI	−1.32, −0.79
$CuMesOxaPF_6$	−1.32, −0.80
CoPhPor	−1.77,[a] −1.27,[a] 0.11, 0.76, 0.97
CoPhOxaTFSI	−1.47,[a] −0.91,[a] −0.29,[b] 0.41,[b] 0.82[b]

[a]Cathodic peak potential of the irreversible wave. [b]Quasi-reversible wave.

$TBAPF_6$ and observed two successive reversible redox waves at 0.41 and 0.79 V vs Fc/Fc^+ (Figure 5B), forming porphyrin π-cation radical and dication species, respectively, as reported in the literature.[23,28] The selection of the applied potential in CPE at 0.65 V vs Fc/Fc^+, near the first oxidation of the porphyrin ligand, exhibited a higher % yield in the formation of **CuPhOxaPF$_6$** or **CuPhOxaTFSI**, whereas the selectivity degraded significantly low when the applied potential is more positive than 0.65 V vs Fc/Fc^+ (Table 1). Similarly, CVs collected for **CoPhPor** exhibited two reversible waves at 0.76 and 0.97 V vs Fc/Fc^+ because of the two consecutive $1e^-$ oxidation of the porphyrin ring (Figure 5C).[24,29] **CoPhPor** also exhibited an additional reversible wave at 0.11 V vs Fc/Fc^+ due to the $Co^{II/III}$ redox couple (Figure 5C).[24,30] The highest % yield of **CoPhOxaTFSI**, 73% (Table 1), was only obtained when the applied potential is 0.95 V vs Fc/Fc^+, which is close to the second oxidation of the porphyrin ligand in **CoPhPor**. Together, these results suggest that the application of potential in CPE is crucial to selectively oxidize **CuPhPor** and **CoPhPor** for preparing their verdoheme derivatives.

Structure and Properties of the Biliverdin Derivatives. Yellow-orange rod-shaped crystals of **TriPyOH** were grown by slow diffusion of hexane into $CHCl_3$. The molecular structure is presented in Figure 6A. A disordered $CHCl_3$ molecule is present in the lattice. The conformational disorder is observed in one terminal benzoyl group (C_1−C_6) as well as the ketone oxygen (O_7). The overall structure adopts a U-shaped conformation that may support metal binding via the three pyrrole nitrogen atoms and a benzoyl oxygen to form a (3N + O) coordination motif, provided a 78° rotation occurs about the C_{25}−C_{32} bond to bring the N_{36} pyrrole ring in-plane with the remaining pyrrole groups (Figure 6B).

Furthermore, density functional theory calculations using the B3LYP method and 6-311++g(d,p) basis set were carried out to obtain the optimized structure of **TriPyOH** (Figure 6C).[31−33] The theoretical results are in good agreement with the experimental data. Shinokubo et al. reported CV data of **OEOxaPor** (Figure S11) and its corresponding metal complexes, **MOEOxaPor**, M = Ag, Co, Ni, and Zn (Table S1).[11,34] According to their studies, the first reduction peak (E_{red}^1) of **MOEOxaPor** shows up between −0.66 and −0.91 V vs Fc/Fc^+ regardless of the metal center. It is worth noting that metal-free **OEOxaPor** also exhibits the E_{red}^1 within a similar potential range (Table S1), suggesting that the metal center has minimal influence on the first reduction of the **MOEOxaPor** complexes. These data indicate that the chelating macrocycle ligand mostly influences the electrochemical properties of the metalated 5-oxaporphyrins. To investigate the similar properties in the metal-free verdoheme

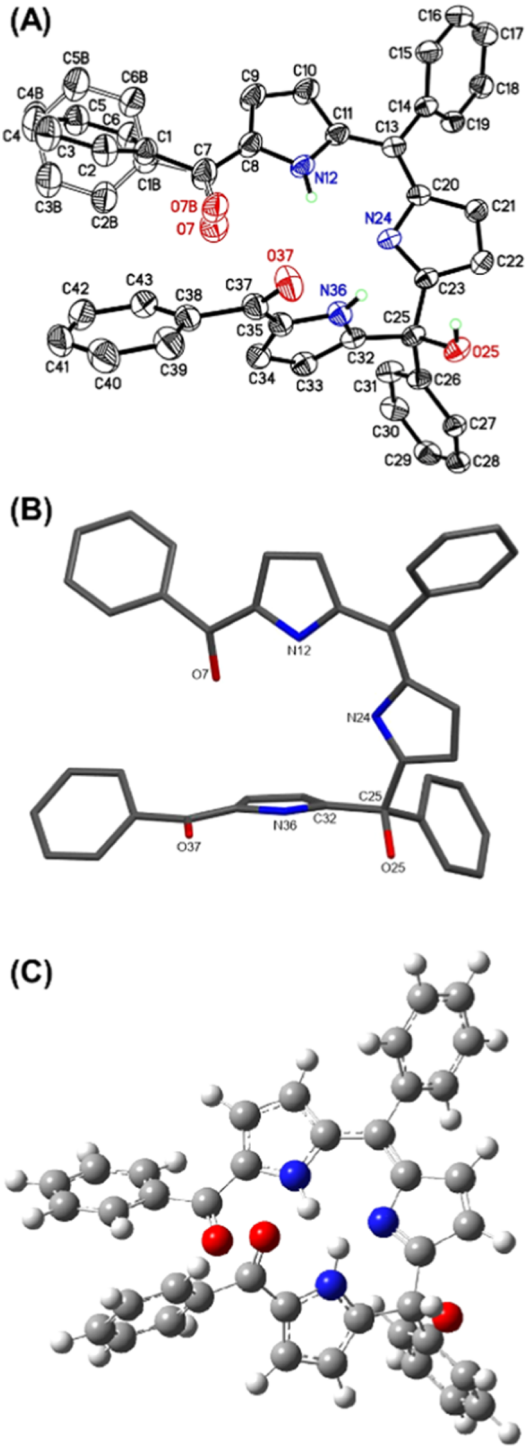

Figure 6. (A) Molecular structure of **TriPyOH**. H atoms bound to carbon and a disordered molecule of chloroform were omitted for clarity. The 50% probability level is set for thermal displacement ellipsoids. (B) Potential metal binding site between the pyrrole rings highlighting the rotation needed for the N_{36} pyrrole ring to be in-plane with the other pyrrole rings. (C) Optimized calculated structure of **TriPyOH** at B3LYP/6-311++g(d,p) level of theory.

compound bearing phenyl groups at the meso positions of the 5-oxaporphyrin ring, **H$_2$PhOxa** (Figure S11) and **CuPhOxaTFSI**, we carried out TD-DFT calculations that elucidated ground and excited state positions for NH cis/trans configurations of **H$_2$PhOxa** macrocycle and **CuPhOxaTFSI**.

https://doi.org/10.1021/jacs.4c02847
J. Am. Chem. Soc. 2024, 146, 15955−15964

These included both NH isomeric forms of **H_2PhOxa** due to two distinct NH tautomeric states within the macrocycle, as reported by Shinokubo et al.[11,34] Energy-level analysis assessed ground (S_0) and excited (S_1, S_2, and S_3) states, showing good correlation with experimental data. Results including HOMO and LUMO molecular orbitals (MOs) are tabulated (Table S2) and graphically presented (Figure S12). MO analysis revealed similar energy levels and gaps for ground and excited states, suggesting minimal influence of the Cu center on the first reduction.[35] Furthermore, the calculated UV−vis spectra of **CuPhOxa** show a good correlation with experimental data in which the lowest excitation bands were assigned as the HOMO/LUMO transition with f = 0.1923 at 556 nm (Figure S13).

EXPERIMENTAL SECTION

Electrosynthesis. Electrosynthesis experiments were carried out in a split H-cell with a glass frit separating the working and counter cells as well as in an undivided cell. Pt mesh working electrode, carbon rod counter electrode, and nonaqueous $Ag/AgNO_3$ (0.01 M) reference electrode were used for all electrochemical experiments. In the H-cell with glass frit, electrolysis was performed using 2.5 mM **CuPhPor** (Figure S14), **CoPhPor** (Figure S15), or **H_2PhPor** (Figure S16) in MeCN or CH_2Cl_2 (10 mL) solution at the working cell vs blank solution at the counter cell. Two stir bars were used for vigorously stirring both cells while exposing them to air. Different potentials and timing were used for each compound. After electrolysis, the electrolyte solution was dried using a rotavap and high-pressure vacuum. LiTFSI was removed by washing three times with distilled water and extracting with CH_2Cl_2. In addition, the $TBAPF_6$ residue was washed and filtered using diethyl ether. Silica gel column chromatography was used for the isolation and purification of products using 10−20% EtOAc in CH_2Cl_2 as the eluent. However, all electro-synthesized and isolated verdoheme derivatives have good solubility in most organic solvents, including dichloromethane, chloroform, MeCN, acetone, ethyl acetate, and diethyl ether but decomposed in alcohols and DMF to form linear tetrapyrroles.[12]

[*meso*-Triphenyl-21,23-didehydro-23*H*-5-oxaporphyrinato]-copper(II) (CuPhOxaPF_6 and CuPhOxaTFSI). A sample of **CuPhPor** (17 mg, 0.025 mmol) was dissolved in 0.1 M $TBAPF_6$ for **CuPhOxaPF_6** or LiTFSI for **CuPhOxaTFSI** MeCN (10 mL) in the working cell. The electrolysis was performed at 0.65 V over 8 h, and the products were separated using column chromatography. **CuPhOxaPF_6**. Yield: 12 mg, 63%. ESI-MS obsd 602.1163, calcd 602.1162 ([M], M = $C_{37}H_{23}CuN_4O^+$); UV−visible (CH_2Cl_2, 25 °C): λ_{max} (ε_{max}) 299 (1.35×10^4), 390 (2.31×10^4), 649 (3.12×10^4). **CuPhOxaTFSI**. Yield: 18 mg, 82%. ESI-MS obsd 602.1169, calcd 602.1162 ([M], M = $C_{37}H_{23}CuN_4O^+$); UV−visible (CH_2Cl_2, 25 °C): λ_{max} (ε_{max}) 299 (0.91×10^4), 390 (1.92×10^4), 649 (2.07×10^4).

[*meso*-Triphenyl-21,23-didehydro-23*H*-5-oxaporphyrinato]-cobalt(II) (CoPhOxaTFSI). A sample of **CoPhPor** (16.8 mg, 0.025 mmol) was dissolved in 0.1 M LiTFSI MeCN (10 mL) in the working cell. The electrolysis was performed at 0.95 V vs Fc/Fc^+ over 8 h. Yield: 16 mg, 73%. ^{1}H NMR (400 MHz, $CDCl_3$), δ 4.75 (s, 1H), 6.21 (t, J = 4.0 Hz, 1H), 6.38 (d, J = 4.0 Hz, 1H), 6.56 (d, J = 4.0 Hz, 1H), 6.81−6.86 (m, 2H), 6.87 (d, J = 4.0 Hz, 1H), 7.31−7.64 (m, 16H), 7.87 (d, J = 4.0 Hz, 2H), 7.91 (d, J = 4.0 Hz, 2H), 9.88 (s, 1H), 12.61 (br, 1H); ^{13}C NMR (100 MHz, $CDCl_3$), δ 13.40, 19.41, 23.65, 58.46, 114.62, 127.62, 128.56, 129.45, 129.83, 130.48, 135.86; ESI-MS obsd 598.1187, calcd 598.1204 ([M], M = $C_{37}H_{23}CoN_4O^+$); UV−visible (CH_2Cl_2, 25 °C): λ_{max} (ε_{max}) 300 (1.6×10^4), 411 (4.52×10^4), 649 (2.02×10^4).

[*meso*-Trimesityl-21,23-didehydro-23*H*-5-oxaporphyrinato]copper(II) (CuMesOxaTFSI and CuMesOxaPF_6). A sample of **CuMesPor** (21.10 mg, 0.025 mmol) was dissolved in 0.1 M LiTFSI for **CuMesOxaTFSI** and $TBAPF_6$ for **CuMesOxaPF_6** MeCN (10 mL) in the working cell. The electrolysis was performed at 0.85 V over 8 h. **CuMesOxaTFSI**. Yield: 17 mg, 67%. HR-MS obsd 728.2552, calcd 728.2576 ([M], M = $C_{46}H_{41}CuN_4O^+$); UV−vis (CH_2Cl_2, 25 °C): λ_{max} (ε_{max}) 304 (2.58×10^4), 385 (3.13×10^4), 653 (3.15×10^4). **CuMesOxaPF_6**. Yield: 14 mg, 64%. ESI-MS obsd 728.2558, calcd 728.2576 ([M], M = $C_{46}H_{41}CuN_4O^+$); UV−visible (CH_2Cl_2, 25 °C): λ_{max} (ε_{max}) 304 (1.53×10^4), 385 (1.91×10^4), 653 (1.85×10^4).

TriPyOH. A sample of **H_2PhPor** (15.50 mg, 0.025 mmol) was dissolved in the working cell electrolyte. The electrolysis was performed at 1.8 V vs Fc/Fc^+ over 18 h. The product was purified using column chromatography with 10% ethyl acetate in CH_2Cl_2 as the eluent. Yield: 0.12 g, 79%. ^{1}H NMR (400 MHz, $CDCl_3$), δ 4.75 (s, 1H), 6.21 (t, J = 4.0 Hz, 1H), 6.38 (d, J = 4.0 Hz, 1H), 6.56 (d, J = 4.0 Hz, 1H), 6.81−6.86 (m, 2H), 6.87 (d, J = 4.0 Hz, 1H), 7.31−7.64 (m, 16H), 7.87 (d, J = 4.0 Hz, 2H), 7.91 (d, J = 4.0 Hz, 2H), 9.88 (s, 1H), 12.61 (br, 1H); ^{13}C NMR (100 MHz, $CDCl_3$), δ 110.48, 118.49, 120.10, 121.43, 125.07, 126.98, 127.96, 128.24, 128.34, 128.53, 128.00, 129.39, 130.63, 130.81, 131.70, 132.36, 136.27, 136.54, 136.63, 137.48, 137.92, 138.40, 140.30, 141.90, 142.54, 149.94, 176.22, 184.82; ESI-MS obsd 600.2290, calcd 600.2282 ([M + H]$^+$, M = $C_{40}H_{29}N_3O_3$).

X-ray Crystallographic Analysis. X-ray crystallography was used to study the geometry and cation/anion interactions of the prepared oxaporphyrins. Single crystals of **CuPhOxaTFSI** (Figure S17) were obtained by slow diffusion of cyclohexene in a chloroform solution. Crystals of **CoPhOxaTFSI** (Figure S18) and **CuMesOxaPF_6** (Figure S19) were obtained via vapor diffusion of pentane into chloroform. Very tiny, thin, needle-like crystals of **CuMesOxaTFSI** were not suitable for the diffraction experiment, and attempts to obtain single crystals of **CuPhOxaTFSI** were unsuccessful. Crystals of **TriPyOH** (Figure S20) were obtained from $CHCl_3$. Details of the crystallographic experiment, including figures and crystal data tables, are given in the Supporting Information (Tables S3−S9). Full crystallographic details have been deposited with the Cambridge Structural Database, deposition numbers CCDC 2162629−2162631 and 2334682.

CONCLUSIONS

A one-step electrosynthesis protocol was developed for the synthesis of Co and Cu 5-oxaporphyrin complexes bearing pendant phenyl and mesityl meso-substituents and paired with TFSI and PF_6 counteranions. Parameters including the applied potential, electrolysis time, and supporting electrolyte salts were studied to optimize the reaction conditions. In a divided electrolysis cell, the highest yield of 82% was achieved for **CuPhOxaTFSI** using 0.1 M LiTFSI electrolyte solution in the presence of air at a potential of 0.65 V vs Fc/Fc^+ over 8 h. The yield increased to 84% within 5 h using an undivided cell setup. CPE performed under inert conditions did not show product formation, indicating that oxygen is required. X-ray crystallographic analysis revealed coordination of the anion from the LiTFSI electrolyte to the metal center for **CuPhOxaTFSI** and **CoPhOxaTFSI**, whereas no such coordination of the PF_6 anion was observed for **CuMesOxaPF_6**. Furthermore, crystallography showed that the **CuPhOxaTFSI** and **CoPhOxaTFSI** complexes adopt a tetrahedral coordination environment about the metal but a planar arrangement is seen in the **CuMesOxaPF_6** case. Compared to the *meso*-aryl-substituted 5-oxaporphyrin Cu complexes, the absorption profile of the Co complex has different features, indicating the effect of the metal center on the UV−visible spectrum. This facile electrosynthesis methodology opens a new avenue for preparing 5-oxaporphyrins.

ASSOCIATED CONTENT

Supporting Information

The Supporting Information is available free of charge at https://pubs.acs.org/doi/10.1021/jacs.4c02847.

https://doi.org/10.1021/jacs.4c02847
J. Am. Chem. Soc. 2024, 146, 15955−15964

Additional experimental details, methods, electrochemical data, and UV−visible spectra for all compounds (unless not shown herein), and crystallographic data, including parameters (PDF)

Accession Codes

CCDC 2162629−2162631 and 2334682 contain the supplementary crystallographic data for this paper. These data can be obtained free of charge via www.ccdc.cam.ac.uk/data_request/cif, or by emailing data_request@ccdc.cam.ac.uk, or by contacting The Cambridge Crystallographic Data Centre, 12 Union Road, Cambridge CB2 1EZ, UK; fax: +44 1223 336033.

AUTHOR INFORMATION

Corresponding Authors

Soumalya Sinha − *Department of Chemistry, University of Cincinnati, Cincinnati, Ohio 45221, United States;* orcid.org/0000-0002-6212-1102; Email: sinhaso@uc.edu

Jianbing "Jimmy" Jiang − *Department of Chemistry, University of Cincinnati, Cincinnati, Ohio 45221, United States;* orcid.org/0000-0002-7466-522X; Email: jianbing.jiang@uc.edu

Authors

Amir Lashgari − *Department of Chemistry, University of Cincinnati, Cincinnati, Ohio 45221, United States*

Xiao Wang − *Department of Chemistry, University of Cincinnati, Cincinnati, Ohio 45221, United States*

Jeanette A. Krause − *Department of Chemistry, University of Cincinnati, Cincinnati, Ohio 45221, United States*

Complete contact information is available at: https://pubs.acs.org/10.1021/jacs.4c02847

Author Contributions

The manuscript was written through contributions of all authors.

Notes

The authors declare no competing financial interest.

ACKNOWLEDGMENTS

This study was supported by the National Science Foundation under grant no. CHE-2041436. Funding for the Bruker D8 Venture diffractometer and the Bruker AVANCE NEO 400 MHz NMR spectrometer was provided through NSF-MRI grants CHE-1625737 and CHE-1726092, respectively.

REFERENCES

(1) Matano, Y. Synthesis of Aza-Oxa-and Thiaporphyrins and Related Compounds. *Chem. Rev.* **2017**, *117* (4), 3138−3191.

(2) Roelfes, G. Repurposed and Artificial Heme Enzymes for Cyclopropanation Reactions. *J. Inorg. Biochem.* **2021**, *222*, 111523.

(3) Sinha, S.; Williams, C. K.; Jiang, J. Outer-Coordination Sphere in Multi-H^+/Multi-e^- Molecular Electrocatalysis. *iScience* **2022**, *25* (1), 103628.

(4) Maines, M. D. Heme Oxygenase: Function, Multiplicity, Regulatory Mechanisms, and Clinical Applications. *FASEB J.* **1988**, *2* (10), 2557−2568.

(5) Wilks, A. Heme Oxygenase: Evolution, Structure, and Mechanism. *Antioxid. Redox Signaling* **2002**, *4* (4), 603−614.

(6) Elbirt, K. K.; Bonkovsky, H. L. Heme Oxygenase: Recent Advances in Understanding Its Regulation and Role. *Proc. Assoc. Am. Physicians* **1999**, *111* (5), 438−447.

(7) Yoshida, T.; Migita, C. T. Mechanism of Heme Degradation by Heme Oxygenase. *J. Inorg. Biochem.* **2000**, *82* (1−4), 33−41.

(8) Mathew, L. G.; Beattie, N. R.; Pritchett, C.; Lanzilotta, W. N. New Insight into the Mechanism of Anaerobic Heme Degradation. *Biochemistry* **2019**, *58* (46), 4641−4654.

(9) Saito, S.; Itano, H. A. Cyclization of Biliverdins to Verdohaemochromes. *J. Chem. Soc., Perkin Trans. 1* **1986**, 1.

(10) Balch, A. L.; Mazzanti, M.; St. Claire, T. N.; Olmstead, M. M. Production of Oxaporphyrin and Biliverdin Derivatives by Coupled Oxidation of Cobalt(II) Octaethylporphyrin. *Inorg. Chem.* **1995**, *34* (8), 2194−2200.

(11) Takiguchi, A.; Kang, S.; Fukui, N.; Kim, D.; Shinokubo, H. Dual Emission of a Free-Base 5-Oxaporphyrinium Cation from Its Cis- and Trans-NH Tautomers. *Angew. Chem., Int. Ed.* **2021**, *60* (6), 2915−2919.

(12) Kakeya, K.; Nakagawa, A.; Mizutani, T.; Hitomi, Y.; Kodera, M. Synthesis, Reactivity, and Spectroscopic Properties of Meso-Triaryl-5-Oxaporphyrins. *J. Org. Chem.* **2012**, *77* (15), 6510−6519.

(13) Sun, Z.-C.; She, Y.-B.; Zhou, Y.; Song, X.-F.; Li, K. Synthesis, Characterization and Spectral Properties of Substituted Tetraphenylporphyrin Iron Chloride Complexes. *Molecules* **2011**, *16* (4), 2960−2970.

(14) Chizhova, N. V.; Kumeev, R. S.; Mamardashvili, N. Zh. Synthesis and Spectral Properties of Cobalt(II) and Cobalt(III) Tetraarylporphyrinates. *Russ. J. Inorg. Chem.* **2013**, *58* (6), 740−743.

(15) Gryko, D.; Lindsey, J. S. Rational Synthesis of Meso-Substituted Porphyrins Bearing One Nitrogen Heterocyclic Group. *J. Org. Chem.* **2000**, *65* (7), 2249−2252.

(16) Yamauchi, T.; Mizutani, T.; Wada, K.; Horii, S.; Furukawa, H.; Masaoka, S.; Chang, H.-C.; Kitagawa, S. A Facile and Versatile Preparation of Bilindiones and Biladienones from Tetraarylporphyrins. *Chem. Commun.* **2005**, No. 10, 1309.

(17) Nakamura, R.; Kakeya, K.; Furuta, N.; Muta, E.; Nishisaka, H.; Mizutani, T. Synthesis of Para- or Ortho-Substituted Triarylbilindiones and Tetraarylbiladienones by Coupled Oxidation of Tetraarylporphyrins. *J. Org. Chem.* **2011**, *76* (15), 6108−6115.

(18) Rafiee, M.; Mayer, M. N.; Punchihewa, B. T.; Mumau, M. R. Constant Potential and Constant Current Electrolysis: An Introduction and Comparison of Different Techniques for Organic Electrosynthesis. *J. Org. Chem.* **2021**, *86* (22), 15866−15874.

(19) Rafiee, M.; Abrams, D. J.; Cardinale, L.; Goss, Z.; Romero-Arenas, A.; Stahl, S. S. Cyclic Voltammetry and Chronoamperometry: Mechanistic Tools for Organic Electrosynthesis. *Chem. Soc. Rev.* **2024**, *53* (2), 566−585.

(20) Chaturvedi, A.; Williams, C. K.; Devi, N.; Jiang, J. Effects of Appended Poly(Ethylene Glycol) on Electrochemical CO_2 Reduction by an Iron Porphyrin Complex. *Inorg. Chem.* **2021**, *60* (6), 3843−3850.

(21) Sinha, S.; Warren, J. J. Unexpected Solvent Effect in Electrocatalytic CO_2 to CO Conversion Revealed Using Asymmetric Metalloporphyrins. *Inorg. Chem.* **2018**, *57* (20), 12650−12656.

(22) Liu, Y.; Moënne-Loccoz, P.; Loehr, T. M.; De Montellano, P. R. O. Heme Oxygenase-1, Intermediates in Verdoheme Formation and the Requirement for Reduction Equivalents. *J. Biol. Chem.* **1997**, *272* (11), 6909−6917.

(23) Ye, L.; Ou, Z.; Fang, Y.; Xue, S.; Song, Y.; Wang, L.; Wang, M.; Kadish, K. M. Electrochemistry of nonplanar copper(ii) tetrabutano- and tetrabenzotetraarylporphyrins in nonaqueous media. *RSC Adv.* **2015**, *5* (94), 77088−77096.

(24) Ye, L.; Fang, Y.; Ou, Z.; Xue, S.; Kadish, K. M. Cobalt Tetrabutano- and Tetrabenzotetraarylporphyrin Complexes: Effect of Substituents on the Electrochemical Properties and Catalytic Activity of Oxygen Reduction Reactions. *Inorg. Chem.* **2017**, *56* (21), 13613−13626.

(25) Fleischer, E. B. The Structure of Copper Tetraphenylporphine. *J. Am. Chem. Soc.* **1963**, *85* (9), 1353−1354.

(26) Li, X. Y.; Nie, J. Density Functional Theory Study on Metal Bis(Trifluoromethylsulfonyl)Imides: Electronic Structures, Energies,

Catalysis, and Predictions. *J. Phys. Chem. A* **2003**, *107* (31), 6007−6013.
(27) Earle, M. J.; Hakala, U.; McAuley, B. J.; Nieuwenhuyzen, M.; Ramani, A.; Seddon, K. R. Metal Bis{(Trifluoromethyl)Sulfonyl}-amide Complexes: Highly Efficient Friedel-Crafts Acylation Catalysts. *Chem. Commun.* **2004**, No. 12, 1368−1369.
(28) Saphier, M.; Yifrah, T.; Zilbermann, I.; Saphier, O.; Shames, A. I.; Froumin, N.; Meyerstein, D.; Guldi, D. M. The Redox Chemistry of Copper Tetraphenylporphyrin Revisited. *J. Porphyrins Phthalocyanines* **2012**, *16* (10), 1124−1131.
(29) Truxillo, L. A.; Davis, D. G. Electrochemistry of Cobalt Tetraphenylporphyrin in Aprotic Media. *Anal. Chem.* **1975**, *47* (13), 2260−2267.
(30) D'Souza, F.; Villard, A.; Van Caemelbecke, E.; Franzen, M.; Boschi, T.; Tagliatesta, P.; Kadish, K. M. Electrochemical and spectroelectrochemical behavior of cobalt(III), cobalt(II), and cobalt(I) complexes of meso-tetraphenylporphyrinate bearing bromides on the .beta.-pyrrole positions. *Inorg. Chem.* **1993**, *32* (19), 4042−4048.
(31) Shimada, K.; Mizutani, T. Synthesis and Reactivity of 10,15,20-Triaryl-5-Oxaporphyrin Copper Complexes. *Tetrahedron Lett.* **2022**, *103*, 153977.
(32) Radoń, M.; Broclawik, E.; Pierloot, K. DFT and Ab Initio Study of Iron-Oxo Porphyrins: May They Have a Low-Lying Iron(V)-Oxo Electromer? *J. Chem. Theory Comput.* **2011**, *7* (4), 898−908.
(33) Frisch, M. J.; Trucks, G. W.; Schlegel, H. B.; Scuseria, G. E.; Robb, M. A.; Cheeseman, J. R.; Scalmani, G.; Barone, V.; Petersson, G. A.; Nakatsuji, H.; Li, X.; Caricato, M.; Marenich, A. V.; Bloino, J.; Janesko, B. G.; Gomperts, R.; Mennucci, B.; Hratchian, H. P.; Ortiz, J. V.; Izmaylov, A. F.; Sonnenberg, J. L.; Williams-Young, D.; Ding, F.; Lipparini, F.; Egidi, F.; Goings, J.; Peng, B.; Petrone, A.; Henderson, T.; Ranasinghe, D.; Zakrzewski, V. G.; Gao, J.; Rega, N.; Zheng, G.; Liang, W.; Hada, M.; Ehara, M.; Toyota, K.; Fukuda, R.; Hasegawa, J.; Ishida, M.; Nakajima, T.; Honda, Y.; Kitao, O.; Nakai, H.; Vreven, T.; Throssell, K.; Montgomery, J. A., Jr.; Peralta, J. E.; Ogliaro, F.; Bearpark, M. J.; Heyd, J. J.; Brothers, E. N.; Kudin, K. N.; Staroverov, V. N.; Keith, T. A.; Kobayashi, R.; Normand, J.; Raghavachari, K.; Rendell, A. P.; Burant, J. C.; Iyengar, S. S.; Tomasi, J.; Cossi, M.; Millam, J. M.; Klene, M.; Adamo, C.; Cammi, R.; Ochterski, J. W.; Martin, R. L.; Morokuma, K.; Farkas, O.; Foresman, J. B.; Fox, D. J. *Gaussian*; Gaussian, Inc: Wallingford CT, 2016.
(34) Takiguchi, A.; Sakakibara, E.; Sugimoto, H.; Shoji, O.; Shinokubo, H. A Heme-Acquisition Protein Reconstructed with a Cobalt 5-Oxaporphyrinium Cation and Its Growth-Inhibition Activity Toward Multidrug-Resistant Pseudomonas Aeruginosa. *Angew. Chem., Int. Ed.* **2022**, *61* (7), No. e202112456.
(35) Giraudeau, A.; Louati, A.; Gross, M.; Callot, H. J.; Hanson, L. K.; Rhodes, R. K.; Kadish, K. M. Reduction of Copper Tetracyanotetraphenylporphyrin in Nonaqueous Media - Formation of Copper(I). *Inorg. Chem.* **1982**, *21* (4), 1581−1586.

https://doi.org/10.1021/jacs.4c02847
J. Am. Chem. Soc. 2024, 146, 15955−15964